World Applied Sciences Journal 32 (6): 1074-1086, 2014
ISSN 1818-4952

DOI: 10.5829/idosi.wasj.2014.32.06.1902

A Numerical Simulation of Unsteady Flow in a Quasi-Seesaw Glottal Model

Tahir Mushtaq Qureshi and Khalid Saifullah Syed

Center for Advance Studies in Pure and Applied Mathematics (CASPAM)
Bahauddin Zakariya University, Multan, Pakistan

Abstract: We present a model for forced oscillatory motion of vocal folds. In this model, we incorporate oscillatory motion of the glottis by considering the moments of glottis about its fulcrum point which is very similar to seesaw motion. By changing the position of the fulcrum point, we can have different scenarios for the motion of the glottis. Forced oscillatory motion of vocal folds, together with the solution of Navier-Stokes equations, approximates the flow within an idealized human glottis. Typical results are obtained by considering Reynolds number 1000 for the cases when fulcrum point is in the middle of the glottis and when it divides the glottis in the ratio 1:3. Fulcrum point plays a pivotal role in determining the characteristics of glottal flow. It has strong effect on the central pressure and axial velocity profiles, cross-sectional velocity profiles at the inlet, outlet and within the glottal constriction and formation and structure of vortices in the glottal flow. When the fulcrum point is located nearer the entry section, amplitude of the forward flow at the entry decreases, reverse flow at the outlet is reduced, jet flow is smoothed out at the outlet and flow separation locations are concentrated at the exit.

Key words: Quasi-seesaw glottal model · Unsteady flow · Vocal folds · Jet flow · Separation locations

INTRODUCTION

Vibration of the vocal folds plays a central role in the production of human voice. A mathematical and numerical model could be very helpful in the study of laryngeal aerodynamics. Due to flow-induced vibration of the vocal fold is, computational simulations of vocal fold oscillation include h airflow and tissue dynamics models.

The simplest models are one- and two-mass models which were presented by Flanagan and Landgraf and Ishizaka and Flanagan respectively [1, 2]. These models are assumed to be one dimensional, inviscid and quasi-steady so that the Bernoulli's law can be applied. Many improvements and variations to these models have been employed in [3-8].

Some important effects such as flow separation in the glottis [9,10], Coanda effect [11-12], intraglottal pressure and velocity distribution [10, 12-16], glottal airflow rate [10, 17, 18], pulsating air jet flows [19-21] and supraglottal jet turbulence [12] have been studied in higher dimension by means of the computational dynamics. The experimental and numerical results indicate that the airflow can be approximated by boundary layer theory [22] and it is greatly influenced by the wall motion [4, 9] as pressure distribution, friction factor which contribute considerably in the oscillation of the vocal folds.

The behavior of fluid motion in the glottal constriction is looked like incompressible and earlier works show that along with monopole source, a dipole source should have significant importance in the voiced sound production [23]. The sound pressure cannot be estimated well with the Navier-Stokes solvers at low Mach numbers. Alternatively a two step procedure has been reported in [24-25]. The aerodynamic sources are computed in the first step which are, then, used to estimate the propagation and radiation of the sound in the next step. Some effort has been made in compressible form of the Navier-Stokes equations but leads to concern about the order of magnitude between acoustic fluctuations and other variations in the fluid variables [26, 27].

The flow behavior has also been investigated over a wide range of wall-mounted geometries [28-39] and it is shown that the presence of a polyp disrupts the normal

Corresponding Author: Tahir Mushtaq Qureshi, Center for Advance Studies in Pure and Applied Mathematics (CASPAM) Bahauddin Zakariya University, Multan, Pakistan.

flow behavior of the glottal jet throughout the phonatory cycle which has adverse impact on the aerodynamic loadings that drive the vocal fold motion [40].

A number of studies have been focused on the choice of the material properties. For isotropic materials, Poisson's ratios of 0.45 [41], 0.3 [42] and 0.49 [43] have been used in the computational models of the vocal folds. Moreover, a transversely isotropic material model is considered by Tao and Jiang [44-45] and Zheng *et al*. [46]. Recently, the sensitivity of the model motion to the Poisson's ratio have been explored in [47].

As the flow leaves the glottis, it forms a jet in the supra-glottis region. A number studies have also been focused on the air jet flow [12, 19-21, 48-49]. In several works, it has been observed that the glottal jet may vary considerably from one cycle to the next [45-46, 50-54] and has its significant effects on speech production [20, 50-51, 55]. Furthermore, both half-models and full geometrically-symmetric models have also been considered in [26, 41-43, 45, 56-58].

In the present work, we develop a mathematical model for forced oscillation of vocal folds and investigate the effect of seesaw based rotary motion of glottal boundaries on glottal velocity fields and other flow properties. The design and oscillation of glottal surface is an extension of the work presented by Alipour *et al*. in [14]. They employed a forced oscillation model to demonstrate the capability of numerical technique in laryngeal aerodynamics. In their work, the glottal entry diameter was constant with fixed margin line in both directions while the glottal exit diameter was variable with sinusoidal vertical movement of the second margin line. In our work, we incorporate the variable glottal entry and exit diameters by adjusting the horizontal position of first margin line on the medial glottal surface with only one oscillator at the second margin line. By this arrangement, the motion of the glottal surface looks like a seesaw motion in which different horizontal positions of first margin line lead to different scenarios for the motion of the glottis. It also seems to be reasonable to investigate only 2D flow fields because flow field in the glottal region does not change along the anterior-posterior axis. This approach reduces considerable numerical computation. Both vocal folds are assumed to vibrate symmetrically in a regular phonation resulting into further reduction in the computational domain by a factor 1/2. To examine the effects of seesaw like motion of glottal walls on fluid flow, Navier-Stokes equations for incompressible flow are solved numerically by using commercial software Fluent 6.3. Further, profiles of central airflow pressure, central velocity, velocity at the inlet, the fulcrum point and the outlet and flow separation location have also been presented for two different positions of the fulcrum point.

Geometric Description of the Glottal Model: The purpose of this work is to simplify vocal folds tissue mechanics by two dimensional forced oscillation model and to study the airflow through the glottis. Here, the design and temporal deformation of glottal walls is an extension of the work presented by Alipour *et al*. in [14], in which they used constant glottal entry diameter by fixing first margin line at the glottal entry section while the glottal exit diameter was variable due to sinusoidal movement of the second margin line along the vertical direction. In our work, we incorporate variation of both the glottal entry and the exit diameters by introducing a fulcrum point in the glottal surface about which the surface performs forced oscillatory motion due to the vertical sinusoidal movement of only one margin line. The motion of the glottis about its fulcrum point resembles seesaw motion about its fulcrum point. This model may be considered as a generalization of the model proposed by Alipour et. al. [14].

The geometry of the glottal model is shown in Figure 1 as a channel symmetric about its centre line. The length of the channel is L measured parallel to both the plane of symmetry and the direction of airflow while H is the height of the channel G_1 and G_2 are representing the inlet and the outlet locations of the glottal entry and exit sections respectively. The glottal surface is constituted of two sinusoidal curves connected with a straight line segment at the points $(x_1, y_1(t))$ and $(x_2, y_2(t))$ [1]. The surface represented by the line segment between the points $(x_1, y_1(t))$ and $(x_2, y_2(t))$ may be regarded as glottal constriction. Two vertical margin lines are introduced in the model to execute the forced oscillation of the glottal surface and control the amplitude of the entry and exit diameters of the glottis. The margin line H_2 at the exit section of the glottal constriction is fixed horizontally but can perform forced vertical sinusoidal movement with a frequency f. The other margin line H_1 is only horizontally adjustable to change the fulcrum point (x_0, y_0) on the medial glottal surface but fixed vertically. The forced vertical sinusoidal movement of H_2 leads to the quasi-seesaw motion of the glottal surface about its fulcrum point (x_0, y_0). Here, the prefix quasi has two implications. One is that the position of fulcrum point is not fixed rather it is adjustable. The other is that the paths traced by the points $(x_1, y_1(t))$ and $(x_2, y_2(t))$ are assumed to be vertical line segments under the condition

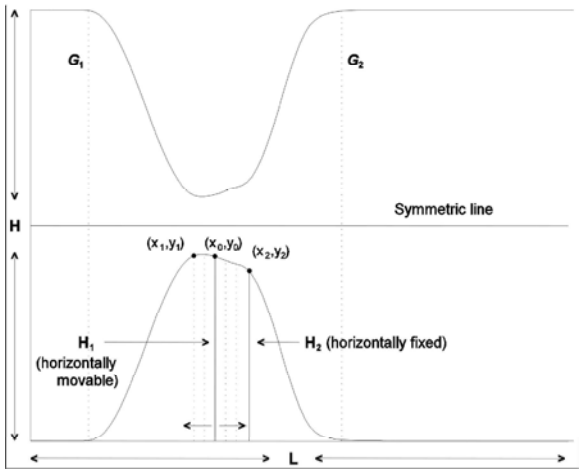

Fig.1: Geometry of the glottal channel.

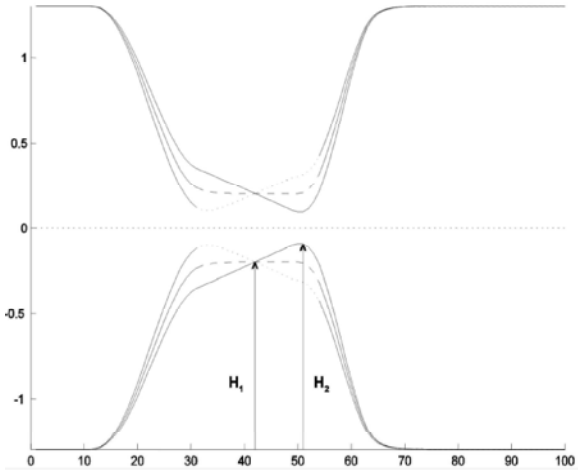

Fig. 2: Schematic animation of glottal surface with fulcrum point at the middle of the glottis.

of sufficiently small amplitude of forced oscillation. These implications follow the horizontally fixed position of H_2 and the variable horizontal position of H_1. The design of present model has an advantage of controlling amplitudes of the entry and the exit diameters of the glottal constriction with only one parameter which is the horizontal position of the fulcrum point. This, in turn, gives control over the extreme values of the constriction entry and exit cross-sectional areas. When the fulcrum point is at the middle of the glottal surface, these amplitudes are same as depicted by Figure 2. When it is moved from the middle position towards the constriction entry section, the amplitude of the entry diameter decreases while that of exit diameter increases as demonstrated in Figure 4. It may be noted that by such variation, minimum cross-sectional area during oscillation at the entry section increases while that at the exit section decreases and that the former remains always greater than the later when the fulcrum point is to the left of the middle point. The extreme case of fulcrum point being at the entry point $(x_1, y_1(t))$, leads to zero amplitude at the entry section while maximum amplitude at the exit section with minimum entry flow area at its maximum value and minimum exit flow area at its minimum value. As the fulcrum point is moved from the entry to the middle point, the above variations go other way round. Similarly, when fulcrum point marches from middle position towards the exit section, the amplitude of the entry diameter begins to increase relative to that of the exit diameter. Furthermore, similar observations can be noticed if we consider that H_1 has vertical sinusoidal movement, fixed at the entry section while H_2 is adjustable along horizontal direction to mark the fulcrum point on the glottis.

Mathematically, we have

$$A(t) = \cos(2\pi ft) \tag{1}$$
$$y_2 = y_0 + BA(t) \tag{2}$$

where y_0 is the mean height, f is the frequency and B is the amplitude. In seesaw motion, both arms of the seesaw have opposite vertical motion with each other and one end is a time delay version of the other end. In the present case, the mean position delay time is $d = \frac{1}{2f}$ as both ends of the seesaw have opposite directions with phase difference of 180°. So,

$$y_1 = y_0 + BA(t - d).$$

Using Eq. (3), we have,

$$y_1 = y_0 - BA(t) \tag{3}$$

Further, suppose that the glottis line is divided in the ratio $m : n$ about the fulcrum point. Then Eqs. (2) and (3) can be rewritten as

$$y_2 = y_0 + mBA(t) \Rightarrow y_2 = y_0 + DA(t) \tag{4}$$
$$y_1 = y_0 - nBA(t) \Rightarrow y_1 = y_0 - EA(t), \tag{5}$$

where $mB = D$ and $nB = E$.

We now demonstrate the oscillation of glottal surface and convergent-divergent configurations of the vocal folds for different positions of the fulcrum point.

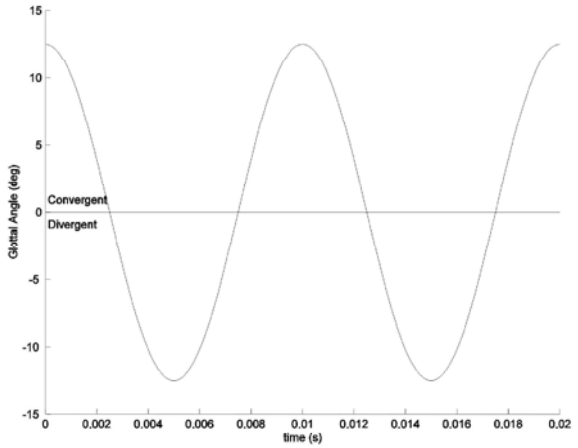

Fig. 3: Convergent (θ>0), parallel (θ=0) and divergent (θ<0) configurations of vocal folds for two cycles of oscillation when the fulcrum point is at the middle of the glottis.

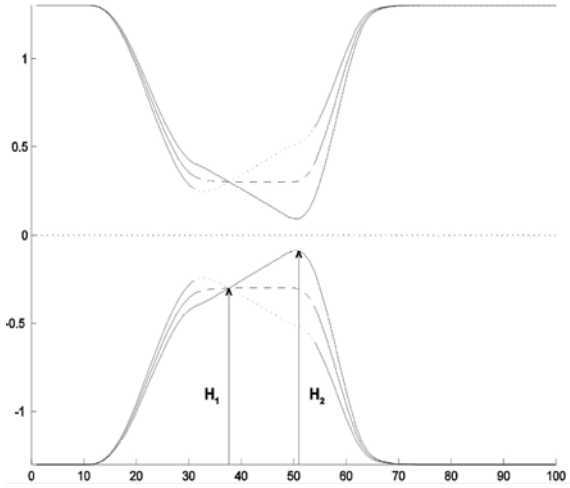

Fig. 4: Schematic animation of glottal surface with fulcrum point dividing the glottis in the ratio 1:3

First, we keep H_1 at the middle of the glottis to mark the position of fulcrum point while H_2 has sinusoidal variation along the vertical direction. During the forced oscillation of H_2 the animation of the glottal surface resembles seesaw motion as shown in Figure 2. Figure 2 also demonstrates that the minimum constriction entry diameter in the extreme divergent configuration is similar to the minimum constriction exit diameter in the extreme convergent configuration. A convergent-parallel-divergent configuration of the present case has been shown in Figure 3. We note that the constriction is convergent when $\theta > 0$, parallel when $\theta = 0$ and divergent when $\theta < 0$.

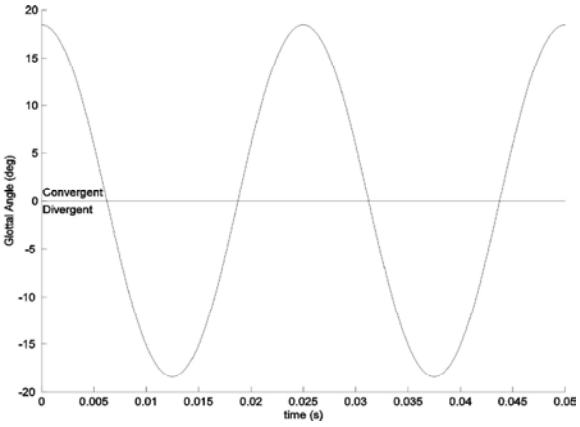

Fig. 5: Convergent (θ>0), parallel (θ=0) and divergent (θ<0) configurations of vocal folds for two cycles of oscillation when the fulcrum point divides the glottis in the ratio 1:3.

As described earlier, by varying the position of the fulcrum point, we have different types of animation patterns of the glottal surface. Figure 4 illustrates the case when the location of fulcrum point is represented by $x_0 - x_1 : x_2 - x_0 = 1:3$ We also note that the minimum entry diameter in the extreme divergent configuration is greater than the minimum exit diameter in the extreme convergent configuration. Figure 5 shows a convergent-parallel-divergent configuration of the present case. Despite its simple design and forced sinusoidal oscillation of only one margin line, both the entry and the exit diameters have been given variation by introducing fulcrum point on the glottis.

Mathematical Model: The governing equations which describe the air flow through larynx are continuity and unsteady Navier-Stokes equations. In the present work, an incompressible, laminar and unsteady airflow has been considered. The laryngeal airflow through small constriction produces jet-like shape, so we can consider this airflow as laminar.

The dimensionless continuity and Navier-Stokes equations are:

$$\nabla \cdot \mathrm{W} = 0, \tag{6}$$

$$\frac{\partial W}{\partial t} + (W \cdot \nabla) W = \frac{1}{\mathrm{Re}} \nabla^2 W - \nabla P, \tag{7}$$

where $W=(U,V)$ is the velocity field, $\mathrm{Re}=\frac{U_0 H}{\nu}$ is the Reynolds number based on the height of the channel H and inlet axial velocity U_0 is the pressure (in Pascal) and t is the time (in seconds).

Numerical Simulation: Geometry of the glottal model was constructed with the help of commercial software GAMBIT. The glottal configuration is symmetric about the centre line as shown in Figure 1. The glottal entry and exit sections have been designed with sinusoidal curves and the constriction entry and exit diameters can have variation from a maximum value of 0.35 cm to a minimum value 0.12 cm during the oscillation. Further, the glottal constriction is constructed by a straight line approximately 0.9 cm in length while half of the height H of the glottal channel is about 1.3 cm. Meshing and specification of boundary types on glottal geometry were performed in the GAMBIT software. This software also allows to export the geometry of the glottal channel with meshing and boundary types in many formats. The unsteady Navier-Stokes equations with glottal geometry were solved using FLUEN which is a commercial CFD software that provides complete mesh flexibility and can solve a very wide variety of flow problems. An export file containing mesh and boundary data was generated by GAMBIT in a format readable by the FLUENT. A UDF (User Define Function) file was created to accommodate the motion of glottal surface. All the necessary operations of loading mesh & UDF files, specifying boundaries, defining fluid properties, executing the solution, refining the mesh and viewing the results were carried out through the graphical user interface of FLUENT.

RESULTS AND DISCUSSION

In the present section, we consider two cases of glottal surface dynamics to study the flow behavior within the constriction: one in which the fulcrum point lies in the middle of the glottis and the other in which the fulcrum point divides the glottal surface in the ratio 1:3. We, first, present our simulation results for the central line pressure and velocity respectively, from the inlet position G_1 to the outlet position G_2 shown in Figure 1. Then, we give the axial velocity profiles at three cross sections, the glottal inlet, the fulcrum point position and the glottal exit respectively. Finally, the flow separation locations with convergent-divergent angle have been shown during two cycles of oscillation. The numerical simulation has been performed with constant inlet flow compatible with constant subglottal pressure and rendering Reynolds number Re = 1000. The frequency f of the oscillator is assumed to be 20 for all the cases considered in the present work. Time step is taken to be uniform and equal to 0.0001 in the time integration of Navier-Stokes equations.

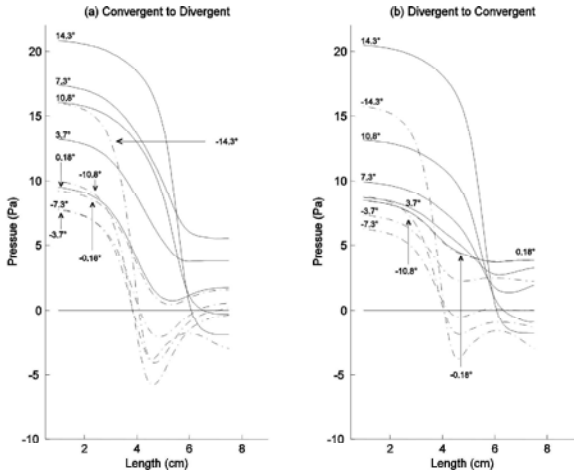

Fig. 6: Central pressure profiles for mid-glottal fulcrum point (a) Central pressure gradient from extreme convergent to extreme divergent configuration, (b) central pressure gradient from extreme divergent to extreme convergent configuration

First of all, we present the central line pressure during one cycle of oscillation for both the cases, separately. We adjust H_1 in such a way that the location of fulcrum point is at the middle of glottis (i.e. $m : n = 1 : 1$) as shown in Figure 2. The oscillation of H_2 generates symmetric motion of glottal surface about its fulcrum point. This motion of glottis is represented by the governing Eqs. (4) and (5) with the assumption that $y_0 = 0.2350$ cm, $D = 0.1150$ and $E = 0.1150$. Figure 6 demonstrates variation of central pressure from inlet of the glottis to the glottal exit marked as G_1 and G_2 respectively in Figure 1. The solid line represents the convergent configuration of vocal folds while dot-dashed line makes their divergent configuration. The legends shown in Figure 6 correspond to the angle of glottal surface, θ. Part (a) corresponds to transition from the extreme convergent to the extreme divergent configuration of vocal folds while part (b) illustrates the transition from the extreme divergent to the extreme convergent configuration. We observe that there is a significant pressure drop near the glottal inlet from the convergent configuration to the divergent one while recovery of pressure occurs from the divergent

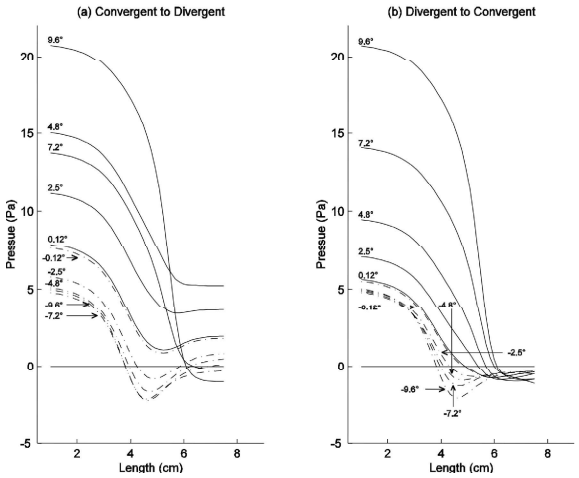

Fig. 7: Central pressure profiles when fulcrum point divides the glottal surface in the ratio 1 : 3 (a) Central pressure gradient from extreme convergent to extreme divergent configuration, (b) central pressure gradient from extreme divergent to extreme convergent configuration.

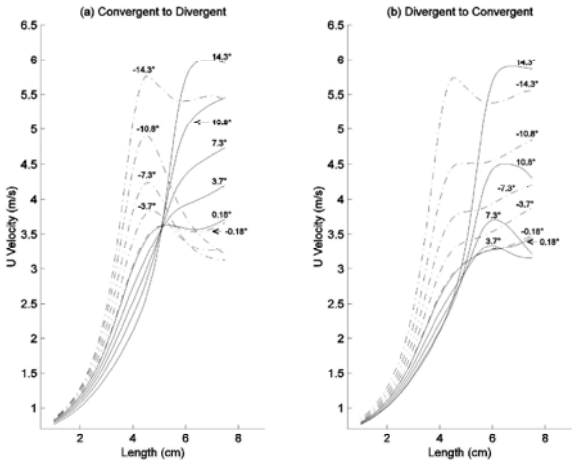

Fig. 8: Central velocity profiles for mid-glottal fulcrum point (a) Central velocity gradient from extreme convergent to extreme divergent configuration, (b) central pressure gradient from extreme divergent to extreme convergent configuration.

configuration to the convergent configuration mainly depending on the motion of glottal surface. Furthermore, there is a lag time of sharp pressure drop and pressure gradient from the extreme convergent to the extreme divergent configurations depending on the minimum cross sectional area during the motion of glottal surface. In the extreme divergent configuration when the minimum cross section area is near the glottal entry, a sharp and early pressure drop occurs near the glottal entry and some recovery of pressure takes place with in the glottis while in the convergent configuration, delayed sharp pressure drop occurs near the glottal exit and no recovery of pressure takes place within the glottis. Figure 6 also indicates that there is negative pressure in both configurations which signifies flow reversal at the separation points due to the motion of glottal wall and constriction of glottis. For the convergent configuration, the reversal occurs for $\theta = 14.3°$ and $\theta = 10.8°$ near the glottal exit in both parts of Figure 6 while for divergent configuration, it occurs within the glottis for all values of θ except $\theta = -0.18°$ in both parts and $\theta = -3.7°$ in part (b).

Figure 7 shows variation of the central pressure from inlet of the glottis to the glottis exit for the case in which fulcrum point divides the glottal surface in the ratio m : $n = 1 : 3$ with $y_0 = 0.2350$ cm, $D = 0.038$ and $E = 0.038$. We note that there is also a considerable pressure drop near the inlet of the glottis but smoother and smaller than that in the previous case. Small recovery of pressure has also been noted from the divergent to the convergent configuration within the glottis. Further, lag time of pressure drop and pressure gradient is lesser than that in the previous case of Figure 6. The Figure 7 further indicates that when the fulcrum point is taken nearer to the entry section, pressure profiles are closely spaced and almost of same shape during the divergent configurations implying smaller variation of pressure in these configurations. Since negative pressure in both configurations points to the flow reversal, we may observe significant decrease in flow reversal in Figure 7 due to change in the fulcrum point location.

Now, we exhibit our results of axial velocity at the central line/line of symmetry of the channel. Figure 8 displays the velocity profiles from inlet of the glottis to glottal exit marked as G_1 and G_2 in Figure 1 when the fulcrum point is taken at the middle of the glottal surface. Solid lines represent the convergent configuration of vocal folds and dot-dashed lines the divergent configuration of vocal folds. The angles displayed at suitable positions represent the legend of the curves. Part (a) corresponds to transition from the extreme convergent to the extreme divergent configuration of vocal fold while part (b) illustrates the transition other way round. Figure 8 illustrates a considerable increase in central axial velocity near the minimum cross sectional area of vocal folds during the oscillation of glottal wall in both configurations. In convergent-divergent configuration, the maximum rise of axial velocity occurs near the

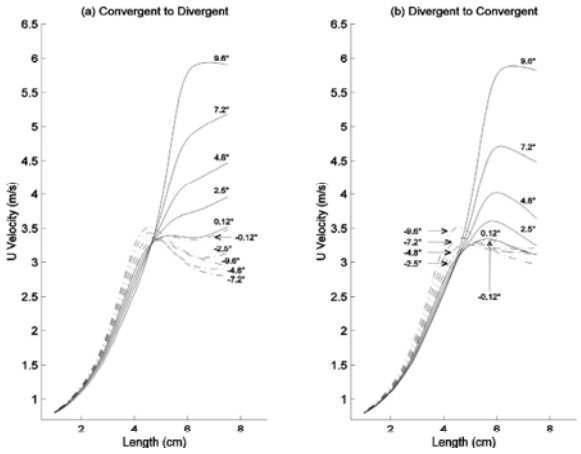

Fig. 9: Central velocity profiles when fulcrum point divides the glottal surface in the ratio 1:3 (a) Central velocity gradient from extreme convergent to extreme divergent configuration, (b) central pressure gradient from extreme divergent to extreme convergent configuration

constriction exit in the extreme convergent case while retardation of axial velocity takes place until a parallel configuration is reached. From parallel to divergent configuration, axial velocity again starts increasing and reaches a maximum value in the extreme divergent near the entry. The figure also depicts the fact that retardation in velocity takes place past the closest part of the constriction of a configuration depending upon the flow reversal pattern in the downstream region. A lag time of position can be observed between the maxima of velocity profiles during the convergent configurations and those of velocity profiles during the divergent configurations.

Figure 9 shows the variation of central velocity from the glottal inlet to the glottal exit in the case when fulcrum point divides the glottal surface in the ratio 1:3. Both parts of Figure 9 illustrate that the velocity profiles of convergent configurations have greater variation near the closest part of the glottal constriction than those of divergent configurations when the fulcrum point is located near the constriction entry. This is in consistent with our previous observation of central pressure profiles for the case under consideration. Further, retardation in all velocity profiles past the closest part of constriction has now decreased with the change in position of the fulcrum point which is in line with the reduction in flow reversal observed in Figure 7. A small lag time of position can also be seen between the maxima of velocity profiles during the convergent configurations and those of velocity profiles during the divergent configurations.

Here, we present in Figure 10 simulation results of axial velocity at glottal inlet, fulcrum point location and glottal outlet for different convergent-divergent configurations of the glottis when the fulcrum point is taken at its middle point. In the current figure, solid lines display the axial velocity profiles in convergent to divergent configurations while dot-dashed lines represent those for divergent to convergent configurations. The legends shown in Figure 10 (a) and 10 (b) correspond to the solid curves in the order from bottom to top and to the dot-dashed curves in the order from top to bottom. In Figure 10 (c), the legends are shown at suitable positions for all the curves. Figure 10 (a) gives the axial velocity profiles at the inlet of the glottis for various values of θ. We can easily view similarity in these profiles. Figure 10 (a) reflects that the peak velocity for every glottal configuration is located at the centre of the inlet to the glottis. Further, the peaks grow higher from convergent to divergent configurations and vice versa. So, the lowest peak occurs in the velocity profile for the extreme convergent case while the highest peak occurs in that for the extreme divergent case. This is due to the fact that the forward flow grows up as the minimum cross section approaches near the inlet. The negative velocity at the sides of velocity profiles indicates flow reversal during the oscillation of glottal surface.

Figure 10 (b) shows the axial velocity profiles within the glottis at the fulcrum point position which is half way the glottal surface. To some extent, dissimilarity with respect to time may be observed in these profiles. It is also notable that the middle part of the velocity profiles tends to be flat no matter whether the configuration is from convergent to parallel or divergent to parallel. Further, small velocity steps have been found on each corner of the profiles. This part also implies that the corners of mid-glottal velocity profiles are rounded in the extreme convergent configuration and advance to flat corners as the configuration tends to be extreme divergent. The steep rise of forward flow in the extreme divergent case indicates the formation of jet like flow which starts to loose from extreme divergent to extreme convergent.

The axial velocity profiles at the outlet of the glottis presented in Figure 10 (c) show that the positive middle velocity peaks are very narrow in width and steep as compared to velocity peaks found in Figure 10 (a) which is the sign of formation of jet-like forward flow. The axial velocity profiles are significantly dissimilar in pattern and have many small velocity steps near the middle velocity peaks. These profiles show complex phenomena and have

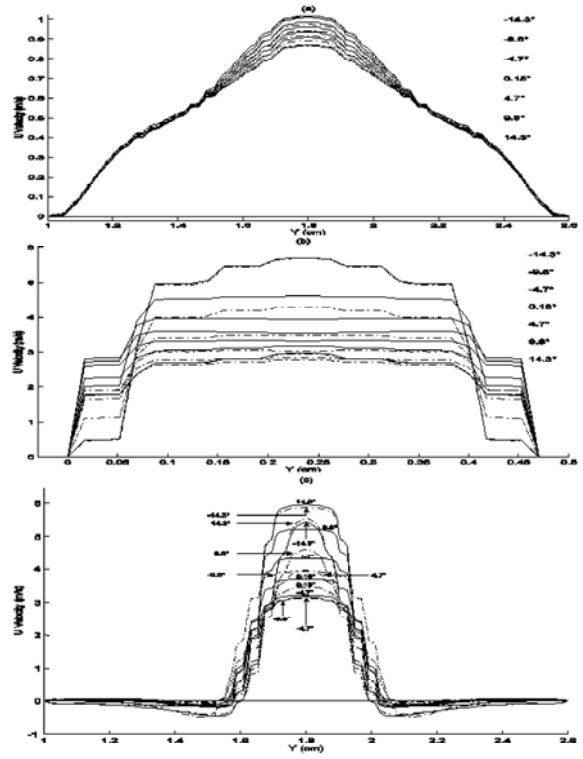

Fig. 10: Axial velocity profiles when fulcrum point is at the middle of the glottis. Parts (a), (b) and (c) correspond to velocity profiles at glottal inlet, fulcrum point location and glottal outlet respectively.

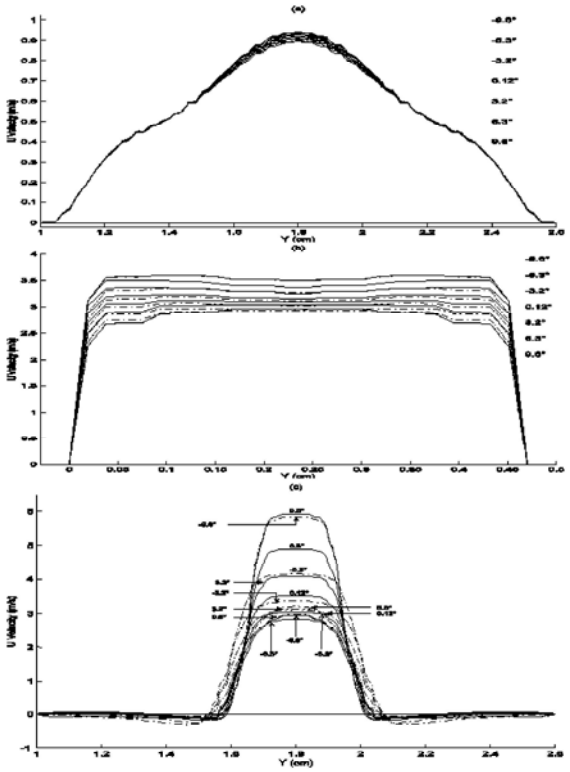

Fig. 11: Axial velocity profiles when fulcrum point divides the glottis in the ratio 1:3. Parts (a), (b) and (c) correspond to velocity profiles at glottal inlet, fulcrum point location and glottal outlet respectively.

many distinctive features than those at the inlet and mid-glottal position presented previously. During the transition from extreme convergent to parallel configuration, the peaks of velocity profiles reduce from the highest value to the lowest value and recover its velocity peaks to some greater extent in parallel to divergent configuration but smaller than the value in the extreme convergent configuration. It may also be noted that the reverse flow exists lateral to the glottal exit due to negative velocity near the corners of positive middle peaks of velocity profiles.

Figure 11 shows axial velocity profiles at the glottal inlet, fulcrum point location and the glottal outlet for the case when the fulcrum point divides the glottis in the ratio 1:3. By comparing Figs. 10 and 11, we may investigate the effect of fulcrum point location on the velocity profiles at the three axial locations, under consideration. A comparison of Figs. 10 (a) and 11 (a) reveals that the difference between the peaks of velocity profiles at the inlet has decreased resulting into smaller amplitude when the fulcrum point is nearer to the inlet. This observation is in line with the reduction of amplitude in the cross-sectional area of the glottis at the inlet with this change in position of fulcrum point already discussed in the context of Figure 4. Moreover, there is an increase in velocity in the vicinity of the side walls at the entry section indicating reduction in flow reversal at the inlet near the walls with change in position of the fulcrum point from the middle towards the entry of the constriction.

From Figure 11 (b), we note in the axial velocity profiles at the current fulcrum point location that there are no small velocity steps on either side of the velocity profiles which results into a longer flat central portion of velocity profiles than in the case of Figure 10 (b). The longer flat central parts of the velocity profiles extended up to the vicinity of walls negate the formation of jet-like flow. The present figure also shows that the corners in velocity profiles are not much rounded in all configurations, in contrast to those in Figure 10 (b). From the convergent to the divergent configuration, the

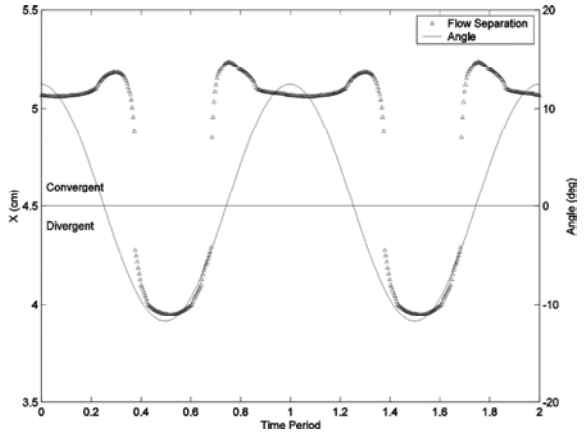

Fig. 12: Convergent-divergent angle shown by solid curve and scaled on the right side of the figure, overlaid with the flow separation locations represented by triangles, scaled on the left side of the figure, for the case of fulcrum point at the middle of the glottis.

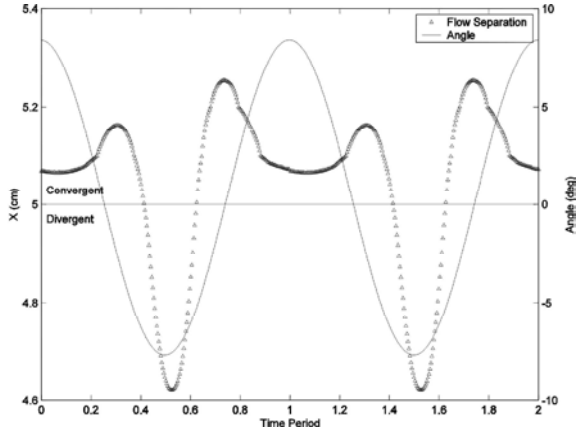

Fig. 13: Convergent-divergent shown by solid curve and scaled on the right side of the figure, overlaid with the flow separation locations represented by triangles, scaled on the left side of the figure, for the case when fulcrum point divides the glottis in the ratio 1:3.

velocity peaks grow in values as the inlet flow increases and gives the largest velocity peak at extreme divergent configuration which is much smaller than that in the case of Figure 10 (b). Similarly, the variation of peaks value of the velocity profiles from the lowest peak to the highest peak is smaller than that of Figure 10 (b).

Figure 11 (c) shows the axial velocity profiles at the outlet of the glottis. Velocity profiles are smoother and more similar than in the case of Figure 10 (c). There are no small velocity steps near positive central peaks of velocity profiles. During the transition from extreme convergent to parallel, same pattern has been observed as in Figure 10 (c) with smooth velocity profiles. But from parallel to extreme divergent, the small amplitudes of recovery of velocity peaks have been viewed. The present part also depicts the flow reversal lateral to glottal exit due to negative velocity near the corners of positive middle peaks of velocity profiles but smaller than that in the case of Figure 10 (c).

Figure 12 gives the graph of flow separation locations represented by triangles, scaled on the left side of the figure overlaid with convergent-divergent configuration angle represented by solid line scaled on the right side of the figure, in the case of fulcrum point being at the middle of the glottis. We notice that the flow separation location is harmonized with the motion of glottal surface. During the convergent configuration of vocal folds (when $\theta > 0$), the flow is separated at the end of the constriction while separation location moves first inward and then outward within the glottis during the divergent configuration (when $\theta < 0$). We observe that the flow separation location resides near the glottal exit constriction about 70% of the cycle.

Figure 13 presents the results of Figure 12 for the case when the fulcrum point resides at the division of glottis in the ratio 1:3. It is notable that the flow separation location remains between the middle and exit constriction of the glottis. There are no sudden large jumps in consecutive flow separation locations as found in Figure 12. We also examine that the flow separation location remains near the glottal exit constriction more than 86% of the cycle, which is greater than that in the case of Figure 12.

Figure 14 displays the flow visualizations for all configurations in one cycle oscillation of vocal folds when the fulcrum point is in the middle of the glottis. The oscillation of glottal wall starts at the extreme convergent configuration of vocal folds and flow passes through the constriction during the extreme convergent to parallel configuration with the time increment. Next, it moves from parallel to divergent configuration and attains its position of being extreme divergent. Vocal folds then, start to move from extreme divergent to parallel configuration. Finally, it acquires the initial position of being extreme convergent after moving from parallel to convergent configuration. We can also examine the flow separation location from glottal wall during the oscillation of vocal folds.

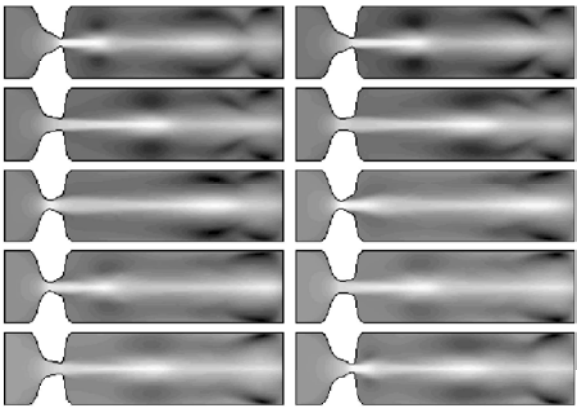

Fig. 14: Glottal axial velocity for different times during one complete cycle of vocal folds for Reynold number 1000 for the case of fulcrum point at the middle of the glottis.

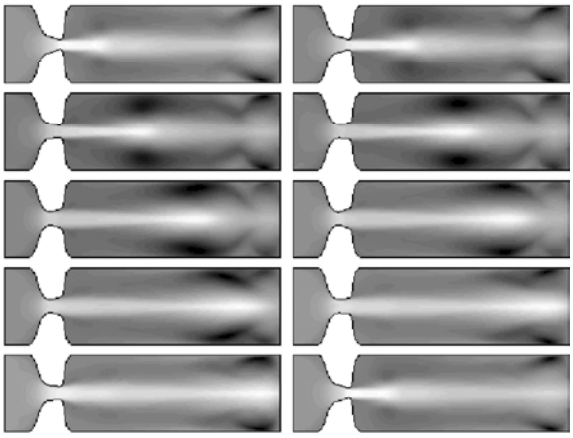

Fig. 15: Glottal axial velocity for different times during one complete cycle of vocal folds for Reynold number 1000 for the case of fulcrum point dividing the glottis in the ratio1:3.

Figure 15 presents flow visualizations for all configurations in one cycle oscillation of vocal folds when the fulcrum point divides the glottis in the ratio 1:3. Same oscillatory pattern has been observed with different separation locations.

CONCLUSIONS

In this work, we have approximated the motion of glottal walls by a seesaw-like motion about its fulcrum point. In this approach, oscillation of one margin line is needed to vary the entry and exit diameters of glottal constriction. Different positions of fulcrum point lead to different scenarios for the motion of glottal walls. We have considered two cases of fulcrum point position, one is assumed in the middle of the glottis while the other is located at the division of the glottis in the ratio 1:3. The numerical experiments have been designed to demonstrate the variability and comparability of pressure and velocity at different positions and cross sections of glottal model to investigate the influence of seesaw-like motion of glottal walls and the position of fulcrum point on these flow variables.

We draw the following conclusions from our observations in the previous section.

- Present results regarding pressure and velocity profiles are physically consistent with each other. This validates our model and the numerical results.
- Glottal boundary deformation can successfully be represented by seesaw-like motion of a flat surface using a fulcrum point and a forced harmonic oscillator.
- Fulcrum point plays a pivotal role in determining the characteristics of the glottal flow. It has strong influence on the central pressure and axial velocity profiles, cross-sectional velocity profiles at the inlet, outlet and within the glottal constriction.
- Fulcrum point may be used to control amplitude of forward flow at the entry, jet-like flow and reverse flow pattern, pressure recovery and flow separation locations within the constriction and at the outlet.
- When the fulcrum point is taken to be nearer the entry section, amplitude of the forward flow at the entry decreases, reverse flow at the outlet is reduced, jet flow is smoothed out at the outlet and flow separation locations are concentrated at the exit.
- Considering the behavior of proposed model, it may be expected that the model will be useful in studying the phenomena of glottal flow, the development of realistic synthesizers and designing the artificial aids.

ACKNOWLEDGEMENTS

The authors of this paper acknowledge the financial support provided by the Higher Education Commission of Pakistan (HEC) under Indigenous Fellowship Scheme.

REFERENCES

1. Flanagan, J.L. and L.L. Landgraf, 1968. Self-oscillating source for vocal tract synthesizers. IEEE Transactions on Audio and Electroacoustics, 16: 57-64.

2. Ishizaka, K. and J.L. Flanagan, 1972. Synthesis of voiced sounds from a two mass model of the vocal cords. Bell System Technical Journal, 51: 1233-1268.
3. Liljencrants, J., 1991. A translating and rotating mass model of the vocal folds. Speech Transmission Laboratory-Quarterly Progress and Status Report, 32: 1-18.
4. Pelorson, X., A. Hirschberg, R. R. van Hassel and A.P.J. Wijnands, 1994. Theoretical and experimental study of quasisteady-flow separation within the glottis during phonation. Application to a modified two mass model. Journal of the Acoustical Society of America, 96: 3416-3431.
5. Story, B.H. and I.R. Titze, 1995. Voice simulation with a body-cover model of the vocal folds. Journal of the Acoustical Society of America, 97: 1249-1260.
6. Herzel, H. and C. Knudsen, 1995. Bifurcations in a vocal fold model. Nonlinear Dynamics, 7: 53-64.
7. Lous, N.J.C., G.C.J. Hofmans, R.N.J. Veldhuis and A. Hirschberg, 1998. A symmetrical two-mass vocal-fold model coupled to vocal tract and trachea, with application to prosthesis design. Acta Acustica (united with Acustica), 84: 1135-1150.
8. De Vries, M.P., H.K. Schutte and G.J. Verkerke, 1999. Determination of parameters for lumped parameter model of the vocal fold using a finite-element method approach. Journal of the Acoustical Society of America, 106: 3620- 3628.
9. Alipour, F. and R.C. Scherer, 2004. Flow separation in a computational oscillating vocal fold model. Journal of the Acoustical Society of America, 116: 1710 -1719.
10. Decker, G.Z. and S.L. Thomson, 2007. Computational simulations of vocal fold vibration: Bernoulli versus Navier-Stokes. Journal of Voice, 21: 273-284.
11. Tao, C., Y. Zhang, D.G. Hottinger and J.J. Jiang, 2007. Asymmetric airflow and vibration induced by the Coanda effect in a symmetric model of the vocal folds. Journal of the Acoustical Society of America, 122: 2270-2278.
12. Suh, J. and S.H. Frankel, 2007. Numerical simulation of turbulence transition and sound radiation for flow through a rigid glottal model. Journal of the Acoustical Society of America, 121: 3728-3739.
13. Guo, C. and R. Scherer, 1993. Finite element simulation of glottal flow and pressure. Journal of the Acoustical Society of America, 94: 688-700.
14. Alipour, F., C. Fan and R.C. Scherer, 1996. A numerical simulation of laryngeal flow in a forced-oscillation glottal model. Computer Speech and Language, 10: 75-93.
15. Li, S., R.C. Scherer, M.X. Wan, S.P. Wang and H.H. Wu, 2006. Numerical study of the effects of inferior and superior vocal fold surface angles on vocal fold pressure distributions. Journal of the Acoustical Society of America, 119: 3003-3010.
16. Punèocháøová-Poøízková, P., K. Kozel and J. Horáèek, 2011. Simulation of unsteady compressible flow in a channel with vibrating walls - Influence of the frequency. Computers & Fluids, 46: 404-410.
17. Duncan, C., G. Zhai and R.C. Scherer, 2006. Modeling coupled aerodynamics and vocal fold dynamics using immersed boundary methods. Journal of the Acoustical Society of America, 120: 2859-2871.
18. Sciamarella, D. and P. Le Quere, 2008. Solving for unsteady airflow in a glottal model with immersed moving boundaries. European Journal of Mechanics B/Fluids, 27: 42-53.
19. Bae, Y. and Y.C. Moon, 2008. Computation of phonation aeroacoustics by an INS/PCE splitting method. Computers & Fluids, 37: 1332-1343.
20. Zheng, X., S. Bielamowicz, H. Luo and R. Mittal, 2009. A computational study of the effect of false vocal folds on glottal flow and vocal fold vibration during phonation. Annals of Biomedical Engineering, 37: 625-642.
21. Larsson, M. and B. Müller, 2009. Numerical simulation of confined pulsating jets in human phonation. Computers & Fluids, 38: 1375-1383.
22. Lagrée, P., Y.E. Berger, M. Deverge, C. Vilain and A. Hirschberg, 2005. Characterization of the pressure drop in a 2d symmetrical pipe: Some asymptotical, numerical and experimental comparisons. ZAMM-Journal of Applied Mathematics and Mechanics/ Zeitschrift für Angewandte Mathematik und Mechanik, 85: 141-146.
23. McGowan, R.S., 1988. An aeroacoustic approach to phonation. Journal of the Acoustical Society of America, 83: 696-704.
24. Oberai, A.A., F. Roknaldin and T.J.R. Hughes, 2000. Computational procedures for determining structural-acoustic response due to hydrodynamic Sources. Computer Methods in Applied Mechanics and Engineering, 190: 345-361.
25. Caro, S., P. Ploumhans, X. Gallez, V. Morgenthaler, G. Mathey, G. Ciapa and J. Ma, 2005. Identification of the appropriate parameters for accurate CAA. In the Proceedings of the 11th AIAA/CEAS Aeroacoustics Conference, Monterey, California, USA, 23-25 May 2005, pp: 2991.

26. Zhao, W., C. Zhang, S. H. Frankel and L. Mongeau, 2002. Computational aeroacoustics of phonation, part i: Computational methods and sound generation Mechanisms. Journal of the Acoustical Society of America, 112: 2134-2146.
27. Zhao, W., C. Zhang, S. H. Frankel and L. Mongeau, 2002. Computational aeroacoustics of phonation, part ii: Effects of flow p arameters and ventricular folds. Journal of the Acoustical Society of America, 112: 2147-2154.
28. Toy, N., W. Moss and E. Savory, 1983. Wind tunnel studies on a dome in turbulent boundary layers. Journal of Wind Engineering and Industrial Aerodynamics, 11: 201-212.
29. Savory, E. and N. Toy, 1986. Hemisphere and hemisphere-cylinders in turbulent boundary layers. Journal of Wind Engineering and Industrial Aerodynamics, 23: 345-364.
30. Savory, E. and N. Toy, 1988. The separated shear layers associated with hemispherical bodies in turbulent boundary layers. Journal of Wind Engineering and Industrial Aerodynamics, 28: 291-300.
31. Acarlar, M.S. and C.R. Smith, 1987. A study of hairpin vortices in a laminar boundary layer. Part 1. Hairpin vortices generated by a hemisphere protuberance. Journal of Fluid Mechanics, 175: 1-41.
32. Tamai, N., T. Asaeda and N. Tanaka, 1987. Vortex structures around a hemispheric hump. Boundary-Layer Meteorology, 39: 301-314.
33. Manhart, M., 1998. Vortex shedding from a hemisphere in a turbulent boundary layer. Theoretical and Computational Fluid Dynamics, 12: 1-28.
34. Sirikci, A., E. Karatas, C. Durucu, T. Baglam, Y. Bayazit, A. Ozkur, S. Sonmezisik and M. Kanlikama, 2007. Noninvasive assessment of benign lesions of vocal folds by means of ultrasonography. Annals of Otology, Rhinology Laryngology, 116: 827-831.
35. Uloza, V., M. Kašë ta, R. Pribuišienë, V. Šaferis, V. Jokû_is, A. Gel_inis and M. Baèauskienë, 2008. Quantitative microlaryngoscopic measurements of vocal fold polyps, glottal gap and their relation to vocal function. Medicina (Kaunas), 44: 266-272.
36. Pattenden, R., S. Turnock and X. Zhang, "Measurements of the flow over a lowaspect-ratio cylinder mounted on a ground plane. Experiments in Fluids, 39: 10- 21.
37. Frederich, O., E. Wassen, F. Thiele, M. Jensch, M. Brede, F. Huttmann and A. Leder, 2008. Numerical simulation of the flow around a finite cylinder with ground plate in comparison to experimental measurements, New Results in Numerical and Experimental Fluid Mechanics VI, Notes on Numerical Fluid Mechanics and Multidisciplinary Design. Springer, Berlin Heidelberg New York, 96: 348-355.
38. Okamoto, S. and N. Uemura, 1991. Effect of rounding side-corners on aerodynamic forces and turbulent wake of a cube placed on a ground plane. Experiments in Fluids, 11: 58-64.
39. Martinuzzi, R., M. AbuOmar and E. Savory, "Scaling of the wall pressure field around surface-mounted pyramids and other bluff bodies. Journal of Fluids Engineering, 129: 1147-1156.
40. Erath, B.D. and M.W. Plesniak, 2012. Three-dimensional laryngeal flow fields induced by a model vocal fold polyp. International Journal of Heat and Fluid Flow, 35: 93-101.
41. Thomson, S., L.L. Mongeau and S.H. Frankel, 2005. Aerodynamic transfer of energy to the vocal folds. Journal of the Acoustical Society of America, 118: 1689-1700.
42. Luo, H., R. Mittal and S.A. Bielamowicz, 2009. Analysis of flow-structure interaction in the larynx during phonation using an immersed-boundary method. Journal of the Acoustical Society of America, 126: 816-824.
43. Smith, S.L. and S.L. Thomson, 2012. Effect of inferior surface angle on the self-oscillation of a computational vocal fold model. Journal of the Acoustical Society of America, 131: 4062-4075.
44. Tao, C. and J.J. Jiang, 2006. Anterior-posterior biphonation in a finite element model of vocal fold vibration. Journal of the Acoustical Society of America, 120: 1570-1577.
45. Tao, C. and J.J. Jiang, 2007. Mechanical stress during phonation in a self-oscillating finite element vocal fold model. Journal of Biomechanics, 40: 2191-2198.
46. Zheng, X., R. Mittal, Q. Xue and S. Bielamowicz, 2011. Direct-numerical simulation of the glottal jet and vocal-fold dynamics in a three-dimensional laryngeal model. Journal of the Acoustical Society of America, 130: 404-415.
47. Shurtz, T.E. and S.L. Thomson, 2012. Influence of numerical model decisions on the flow-induced vibration of a computational vocal fold model. Computers & Structures, 122: 44-54.

48. Schwarze, R., W. Mattheus, J. Klostermann and C. Brücker, 2011. Starting jet flows in a three-dimensional channel with larynx-shaped constriction. Computers & Fluids, 48: 68-83.
49. Krebs, F., F. Silva, D. Sciamarella and G. Artana, 2012. A three-dimensional study of the glottal jet. Experiments in Fluids, 52: 1133-1147.
50. Triep, M., C. Brücker and W. Schröder, 2005. High-speed PIV measurements of the flow downstream of a dynamic mechanical model of the human vocal folds. Experiments in Fluids, 39: 232-245.
51. Zheng, X., R. Mittal and S. Bielamowicz, 2011. A computational study of asymmetric glottal jet deflection during phonation. Journal of the Acoustical Society of America, 129: 2133-2143.
52. Erath, B.D. and M.W. Plesniak, 2006. An investigation of bimodal jet trajectory in flow through scaled models of the human vocal tract. Experiments in Fluids, 40: 683-696.
53. Erath, B.D. and M.W. Plesniak, 2006. An investigation of jet trajectory in flow through scaled vocal fold models with asymmetric glottal passages. Experiments in Fluids, 41: 735-748.
54. Erath, B.D. and M.W. Plesniak, 2010. An investigation of asymmetric flow features in a scaled-up driven model of the human vocal folds. Experiments in Fluids, 49: 131-146.
55. Drechsel, J.S. and S.L. Thomson, 2008. Influence of supraglottal structures on the glottal jet exiting a two-layer synthetic, self-oscillating vocal fold model. Journal of the Acoustical Society of America, 123: 4434-4445.
56. Zheng, X., Q. Xue, R. Mittal and S. Bielamowicz, 2010. A coupled sharp-interface immersed boundary-finite-element method for flow-structure interaction with application to human phonation. Journal of Biomechanical Engineering, 132: 111003.
57. Pickup, B.A. and S.L. Thomson, 2011. Identification of geometric parameters influencing the flow-induced vibration of a two-layer self-oscillating computational vocal fold model. Journal of the Acoustical Society of America, 129: 2121-2132.
58. Zhang, Z., 2009. Characteristics of phonation onset in a two-layer vocal fold model. Journal of the Acoustical Society of America, 125: 1091-1102.